Polymer unfolding and motion synchronization induced by spatially correlated noise

M. Majka* and P. F. Góra
Marian Smoluchowski Institute of Physics, Jagiellonian University, Reymonta 4, 30-059 Kraków, Poland
(Received 14 August 2012; published 19 November 2012)

The problem of a spatially correlated noise affecting a complex system is studied in this paper. We present a comprehensive analysis of a two-dimensional model polymer chain, driven by the spatially correlated Gaussian noise, for which we have varied the amplitude and the correlation length. The chain model is based on a bead-spring approach, enriched with a global Lennard-Jones potential and angular interactions. We show that spatial correlations in the noise inhibit the chain geometry dynamics, enhancing the preservation of the polymer shape. This is supported by the analysis of correlation functions of both the module length and angles between neighboring modules, which have been measured for the noise amplitude ranging over three orders of magnitude. Moreover, we have observed the correlation length dependent bead motion synchronization and the spontaneous polymer unfolding, resulting from an interplay between chain potentials and the spatially structured noise.

DOI: 10.1103/PhysRevE.86.051122 PACS number(s): 05.40.Ca, 36.20.−r, 61.43.Fs, 87.15.A−

I. INTRODUCTION

The understanding of diffusion in complex media is crucial for both modeling conformation transitions in biomolecules and intracellular transport. It is also well known that various systems organize spontaneously in response to random forcing [1] and that the introduction of temporal correlations into the noise can lead to synchronization effects [2]. A well-established framework to simulate these phenomena is provided by Langevin equations, which introduce the concept of stochastic force mimicking the molecular collisions [3]. An important advance in this formalism has been the introduction of the generalized Langevin equation (GLE), which reproduces the anomalous diffusion thanks to the time-correlated stochastic force and the corresponding integral memory kernel, which represents the friction [4]. Recently, Kou [4] derived the GLE from a microscopic model of a particle coupled to a large number of oscillators, thus showing that the particle-environment interaction is essential for the occurrence of temporal correlations in thermal noise. However, it is remarkable that this theory explains solely the temporal aspect of diffusion, while little work has been done to understand its spatial counterpart. This has led us to investigate the problem of a spatially correlated noise affecting a complex system.

The collective media behavior, which is random but characterized by a certain correlation length λ, occurs at a length scale of micrometers in the context of hydrodynamic interactions, e.g., in colloid sedimentation [5,6] or in the study of active particle motion [7]. However, the spatial correlations at the lower length scale play a fundamental role in the theory of phase transitions [8], among which the liquid-glass transition is of special interest. During this transition, the particles suffer a dramatic drop of mobility without the emergence of structural ordering [9]. This phenomenon has been intensively researched for the past two decades, and according to extensive simulations [10,11], it is characterized by the occurrence of spatial correlations in the particles' motion [11], which is recognized as the formation of different-sized clusters [10,12]. Choosing a single moment in time, one could interpret these clusters as a source of a disturbance which is random at the large length scale ($\gg\lambda$) but ordered at the length scale of λ. Figure 1 illustrates this idea. The temporal evolution of this system is still indeterministic, as it "randomly reorders." We propose that this behavior could be imitated by the spatially correlated noise, which is affecting a subsystem, in our case, a model two-dimensional polymeric chain.

We have simulated the chain based on the bead-spring approach under the forcing of spatially correlated Gaussian noise (SCGN) for which we have varied the correlation length and the amplitude. Our previous findings regarding the stiffening of the chain under the SCGN, shown with the aid of the reduced dynamics, have been published in [13]. However, our further investigation into this system, which involves the extension of the parameters' range and the measurements of chain characteristics, has revealed several new effects, namely, bead motion synchronization, increased time correlation of both module length and angles between modules, the inhibition of the average module length growth, and, most notably, the chain unfolding induced by the increased correlation length.

Our simulations are related to the actual physical situation by the choice of λ. Unfortunately, currently, there are few experimentally accessible quantities that describe the collective molecular behavior in the vicinity of the glass transition and can be measured for the variety of temperatures [14]. One of these parameters is the number of cooperatively rearranging molecules [15], which has been reported to increase from 1 in the liquid phase to approximately 10 in the glass phase [15]. Additionally, these results are qualitatively similar for the different chemical compounds [15]. On the other hand, the direct measurements of the correlation length are scarce and limited to a specific experimental setup, as, e.g. in [16], which reports λ to be of the order of two to four molecule diameters. These measurements suggest that λ covering up to five chain nodes is physically meaningful.

This paper has following structure: in Sec. II the methods of the SCGN generation are introduced, and in Sec. III we propose the equations of motion and the correlation function. In Sec. IV we present our polymer model, and Sec. V briefly discusses simulation methods. Sections VI to IX present the

*maciej.majka@uj.edu.pl

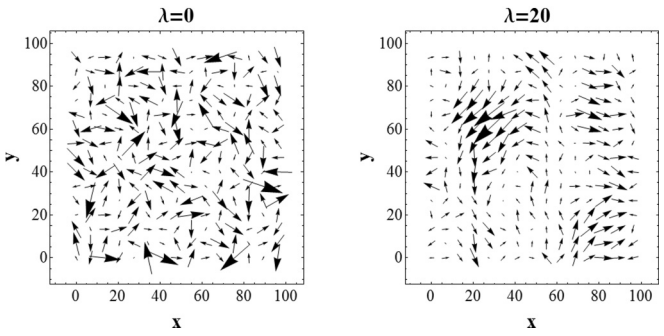

FIG. 1. Spatially correlated random vectors with correlation length λ, generated on a regular network. For $\lambda = 0$ the pattern is entirely random, but for $\lambda = 20$ the ordered clusters can be noticed.

results regarding each effect with an interpretation, and in Sec. X we summarize our findings.

II. MULTIPLE CORRELATED GAUSSIAN VARIABLES

The generation of multiple correlated Gaussian variables is a central problem in the simulation of SCGN driven systems; therefore we shall outline here the basic algorithm. Let's assume that we have two real vectors of random, zero-mean Gaussian variables, namely, $\vec{\xi}^T = (\xi_1, \ldots, \xi_N)$ and $\vec{\eta}^T = (\eta_1, \ldots, \eta_N)$, whose components satisfy the following correlation relations:

$$\langle \xi_i \xi_j \rangle = S_{ij}, \tag{1}$$

$$\langle \eta_i \eta_j \rangle = \delta_{ij}. \tag{2}$$

Here, δ_{ij} denotes the Kronecker delta, and S_{ij} are elements of the correlation matrix, defined as

$$\langle \vec{\xi} \vec{\xi}^T \rangle = \hat{S}. \tag{3}$$

The matrix $\hat{S}$ is symmetric and positively definite [17], so it is suitable for Cholesky decomposition [18], which factorizes $\hat{S}$ into a lower triangular matrix $\hat{L}$ and its transposition:

$$\hat{S} = \hat{L}\hat{L}^T. \tag{4}$$

The vector of correlated variables $\vec{\xi}$ is related to the uncorrelated vector $\vec{\eta}$ via a linear transformation [19]:

$$\vec{\xi} = \hat{L}\vec{\eta}. \tag{5}$$

This means that, given a correlation matrix, one can generate the correlated Gaussian vector $\vec{\xi}$ simply by sampling N times the normal distribution to obtain the components of $\vec{\eta}$ and then performing the transformation (5).

III. EQUATIONS OF MOTION AND CORRELATION FUNCTION

Our system is equivalent to an ordered set of N interacting material points on a plane, enumerated by the index i. The position of the ith point (or bead, as we will refer to it in the following) is $\vec{r}_i^{\,T} = (x_i, y_i)$. In order to simulate the trajectory $\{\vec{r}_i(t)\}_N$ of the whole system, we have to solve numerically a set of $2N$ stochastic equations of motion:

$$\begin{aligned} m\ddot{x}_i + \gamma \dot{x}_i + \partial_{x_i} U &= \xi_x(\vec{r}_i), \\ m\ddot{y}_i + \gamma \dot{y}_i + \partial_{y_i} U &= \xi_y(\vec{r}_i). \end{aligned} \tag{6}$$

Here, U is the potential energy of the system, which we will discuss in detail in the next section. $\vec{\xi}(\vec{r}_i)^T = [\xi_x(\vec{r}_i), \xi_y(\vec{r}_i)]$ is the two-dimensional SCGN, m is a bead mass, and γ is a friction constant. In the absence of a more relevant theory, we have applied the simplest friction model and have chosen γ to be constant. The differential equations (6) are, in principle, of second order, which we preserve for generality, but in the course of our simulations we have overdamped the system by choosing γ to be large enough.

We assume that the correlation function S_{ij} of stochastic forces acting on beads i and j should depend only on a relative distance between these beads, which is $r_{ij} = |\vec{r}_i - \vec{r}_j|$. Additionally, we assume that there are no cross correlations between the x and y components, which allows us to reduce the correlation relations to the form

$$\begin{aligned} \langle \xi_x(\vec{r}_i)\xi_x(\vec{r}_j)\rangle &= \langle \xi_y(\vec{r}_i)\xi_y(\vec{r}_j)\rangle = S(r_{ij}), \\ \langle \xi_x(\vec{r}_i)\xi_y(\vec{r}_j)\rangle &= 0. \end{aligned} \tag{7}$$

It should be emphasized that the correlation matrix $\hat{S}$ is a dynamical object and evolves in t as the relative distances $r_{ij}(t)$ do. The conditions (7) suggest the following procedure to integrate Eqs. (6): once all beads' positions $\{\vec{r}_i(t)\}_N$ at some moment t are determined, we can calculate the $N \times N$ correlation matrix and its Cholesky decomposition $\hat{L}$; next, according to (5), we shall use $\hat{L}$ and two different $\vec{\eta}$ to obtain $\{\xi_x(\vec{r}_i)\}_N$ and $\{\xi_y(\vec{r}_i)\}_N$. Finally, we can use them to perform an integration step, which gives $\{\vec{r}_i(t + \Delta t)\}_N$. The repeated Cholesky decompositions are the most computationally expansive part of our simulations, as the computational complexity of this decomposition is $O(N^3)$ [18].

Along with conditions (7), we assume that the correlation function S_{ij} is characterized by the correlation length λ, and it reproduces the standard Brownian diffusion for $\lambda \to 0$ [20], so

$$S(r_i(t), r_j(t')) \overset{\lambda \to 0}{=} \frac{2k_B T \gamma}{m} \delta(t - t'). \tag{8}$$

In the above formula k_B denotes the Boltzmann constant and T is temperature. Taking into account (7) and (8), we chose the exponentially decaying spatial correlation function, which resembles the displacement correlation function from [11] and [16]. We also neglect the temporal correlations, as we are interested in the effects of the purely spatially structured noise. Finally, the spatiotemporal correlation function reads

$$S(r_i(t), r_j(t')) = \sigma \frac{\gamma}{m} e^{-\frac{|\vec{r}_i - \vec{r}_j|}{\lambda}} \delta(t - t'), \tag{9}$$

where $\sigma = 2k_B T$ denotes the noise amplitude and we will refer to it as temperature, as it is proportional to the actual physical temperature.

In order to illustrate how the spatial correlations affect the noise pattern, we have applied (5) and (9) to generate the random vectors on a regular network. A snapshot of this simulation is presented in Fig. 1. One can easily notice

clusters of correlated vectors; however, this pattern changes dramatically for every new generation.

IV. THE MODEL OF A POLYMER CHAIN

The polymeric chain is an archetype of many biomolecules; thus we have chosen it as a test object for our simulation. Our model is based on the bead-spring approach, in which i and $i+1$ beads interact with a harmonic potential:

$$U_R = \sum_{i=1}^{N-1} \frac{1}{2} k_1 (|\vec{r}_{i+1} - \vec{r}_i| - d_0)^2. \tag{10}$$

Every bead is also the source of the Lennard-Jones type interaction, which provides the excluded volume effect and

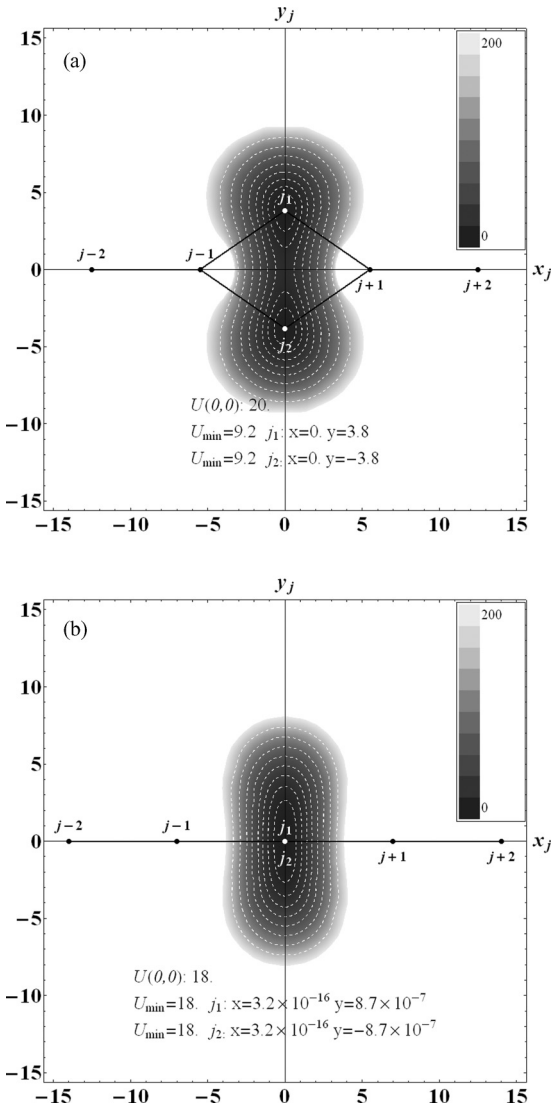

FIG. 2. The energetic landscape for a single bead interacting with its four nearest neighbors. The potential parameters are chosen according to Table I. (a) The distance $|\vec{r}_{j+1} - \vec{r}_{j-1}| = l_0$, and j_1 and j_2 enumerate two possible positions of the jth bead that minimize the potential energy. $U(0,0)$ is the height of the energy barrier, and $U_{\min}$ is the depth of the minimum. (b) The distance $|\vec{r}_{j+1} - \vec{r}_{j-1}| = 1.25 l_0$, and j_1 and j_2 merge into a single minimum as the energy barrier disappears.

TABLE I. The parameters of the system chosen for simulation.

N	k_1	d_0	k_2	l_0	ϵ	σ_{LJ}	γ	m
128	7	7	2	11	1	3	20	1

an interaction between the distant tails of the chain:

$$U_{LJ} = \sum_{i,j}^{N} \epsilon \left(\frac{\sigma_{LJ}^{12}}{|\vec{r}_i - \vec{r}_j|^{12}} - \frac{\sigma_{LJ}^{6}}{|\vec{r}_i - \vec{r}_j|^{6}} \right). \tag{11}$$

Finally, we introduce a harmonic interaction between beads i and $i+2$ which resembles angular interactions:

$$U_\psi = \sum_{i=1}^{N-2} \frac{1}{2} k_2 (|\vec{r}_{i+2} - \vec{r}_i| - l_0)^2. \tag{12}$$

The total potential energy U is equal to

$$U = U_R + U_\psi + U_{LJ}. \tag{13}$$

For $\epsilon = 0$ (no U_{LJ} contribution) the potential energy is minimized when the beads' positions satisfy

$$|\vec{r}_{i+1} - \vec{r}_i| = d_0, \quad |\vec{r}_{i+2} - \vec{r}_i| = l_0. \tag{14}$$

In this case, all of the minimum energy conformations are equienergetic. In fact, unless $l_0 > 2d_0$, once $\vec{r}_1$ and $\vec{r}_2$ are chosen to satisfy $|\vec{r}_2 - \vec{r}_1| = d_0$, the third bead can be positioned in two ways, so the relation $|\vec{r}_3 - \vec{r}_1| = l_0$ is also fulfilled. Successively applying the conditions (14) to the following beads, one can build numerous minimum energy geometries. When $U_{LJ} \neq 0$, the energetic structure of the chain becomes more complex, but if $d_0 > \sigma_{LJ}$ and $\epsilon \simeq k_1$, the Lennard-Jones contribution becomes a perturbation. However, the U_{LJ} influence makes the structures no longer equienergetic.

When the chain's energy is not minimized, the dynamical topography of the potential energy surface depends on both potentials' parameters and the local geometry of the chain. An effective way to represent snapshots of this energy landscape for a single bead is to take into account its four nearest neighbors. An example of such a landscape is reproduced in Fig. 2(a). We have chosen the values of potential energy parameters (Table I) such that the double-minimum structure is distinct and holds for a wide range of local conformations. However, this structure is extremely sensitive to a single parameter, which is the distance $l_j = |\vec{r}_{j+1} - \vec{r}_{j-1}|$. Whenever $l_j > 2d_0$, the two minima tend to merge rapidly into a single one, positioned in line with beads $j-1$ and $j+1$. This is reproduced in Fig. 2(b). This fact significantly affects the high temperature dynamics of the chain, as is show in Sec. IX.

V. SIMULATION

Applying the classical Runge-Kutta method modified for stochastic differential equations [21], we have simulated the system described by Eqs. (6) with the potential (13) and the parameters from Table I. The number of beads has been set to $N = 128$, the bead's mass has been chosen as $m = 1$, and the friction coefficient γ has been set to 20, which overdamped the system.

In our research, we have explored three regimes of temperature. First, we have varied the noise amplitude σ from 0 to 20 units with an interval of 1 unit, and we have increased the correlation length λ from 0 to 20 with an interval of 5 units. In the second regime, we have increased σ from 25 to 250 with an interval of 25 units, and in the third regime we have explored the region from 300 to 1000 units with an interval of 100 units. For the second and the third regimes we have varied λ from 0 to 50 with an interval of 10 units. For each pair of λ and σ we have performed 64 runs, starting from different initial positions. The initial coordinates have been chosen so that the distance between nearest neighbors is equal to d_0, but the angle between modules has been chosen randomly from $\pi/2$ to $3\pi/2$.

The integration step has been set to $1/128$ time unit, and each simulation lasted 2148 time units. The data for the first 100 units have been rejected due to system thermalization. If not stated otherwise, the data have been collected once per time unit. We have gathered the data regarding bead synchronization, module length, and the angle between modules.

VI. THE BEAD MOTION SYNCHRONIZATION

The introduction of the spatial correlations into the noise implies that, at a length scale comparable to the correlation length λ, the stochastic force vectors have similar direction and value. Therefore, one could expect that the motion of beads with a relative distance lower than λ will synchronize. This prediction has been fully confirmed.

As the measure of synchronization at a particular moment t, we have chosen the normalized product of two beads' velocities, distanced by n nodes, which has been averaged along the chain:

$$K_n(t) = \frac{1}{(N-n)} \sum_{i=1}^{N-n} \frac{\vec{v}_i \cdot \vec{v}_{i+n}}{v_i v_{i+n}} = \langle \cos \theta_{i,i+n} \rangle. \qquad (15)$$

Here $\theta_{i,i+n}$ is an angle between velocity vectors of the ith and $(i+n)$th beads. For each run, we have gathered $K_n(t)$, which was time averaged to obtain the synchronization factor K_n. The maximal value of $K_n = 1$ indicates a fully synchronized motion, while $K_n = 0$ implies the opposite.

We have gathered the data for n ranging from 1 to 9. A representative sample of our results is show in Fig. 3. The rise in the synchronization factor K_n along with increasing λ and $\sigma = \text{const}$ is evident. Conversely, the level of synchronization is almost constant for $\lambda = \text{const}$ and varying amplitude, which is valid even for temperatures below $\sigma = 5$. For every n, the factor K_n grows from 0 for $\lambda = 0$ to the maximal observed value for $\lambda = 50$, which is approximately 0.8 for $n = 1$ and 0.3 for $n = 9$.

A further insight into the synchronization comes from the rearrangement of data, so K_n is represented as a function of n, with λ and T being parameters. Figure 4 shows the qualitative similarity between these data for two extreme temperatures ($\sigma = 1$ and $\sigma = 1000$). To obtain a quantitative measure of the decrease in synchronization with the rise in n, we have fitted our data with the exponential decay model:

$$K_n = A_\lambda e^{-B_\lambda n}. \qquad (16)$$

This model proved to be an accurate description of data, as the coefficient of determination R^2 exceeded 0.99 for all fits, except those with $\lambda = 0$, for which $B_{\lambda=0}$ has no physical meaning.

In Fig. 5, we have juxtaposed the values of B_λ for $\sigma \geqslant 25$, at which temperature the behavior of the chain is noise

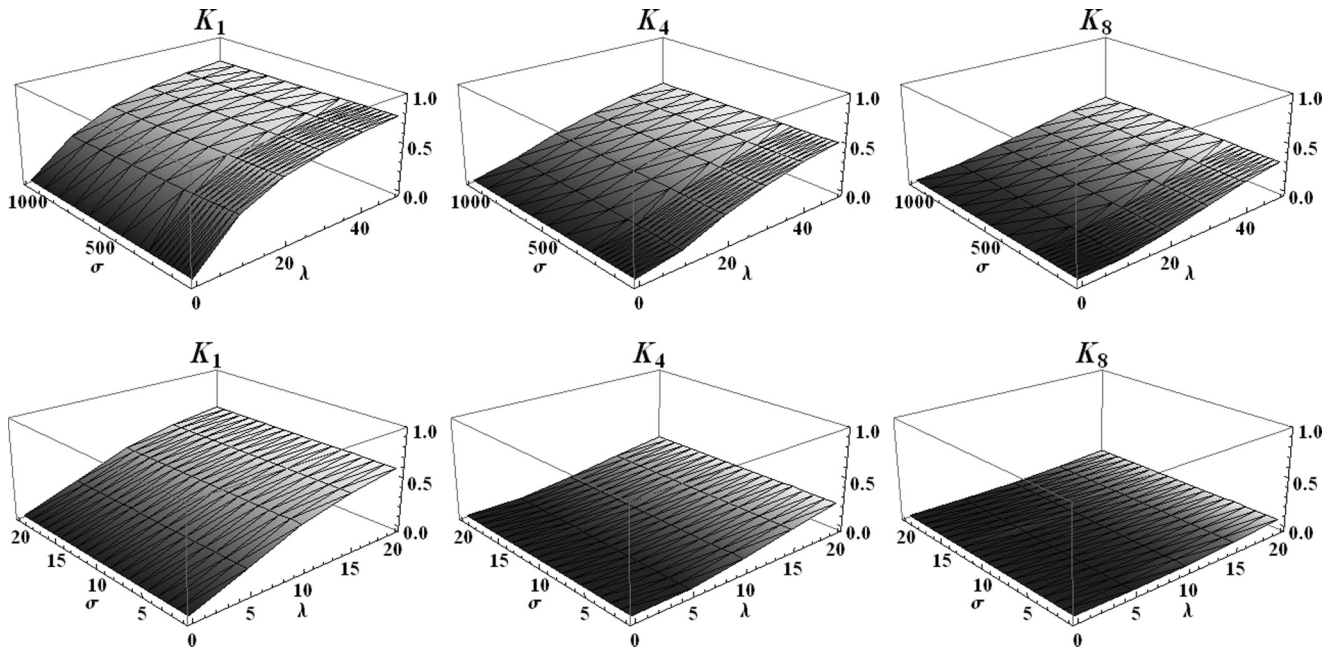

FIG. 3. The synchronization factor K_n for $n = 1,4,8$ as a function of the correlation length λ and the noise amplitude σ. Each column contains the data for the same n in (top) the high temperature regime and (bottom) the low temperature regime.

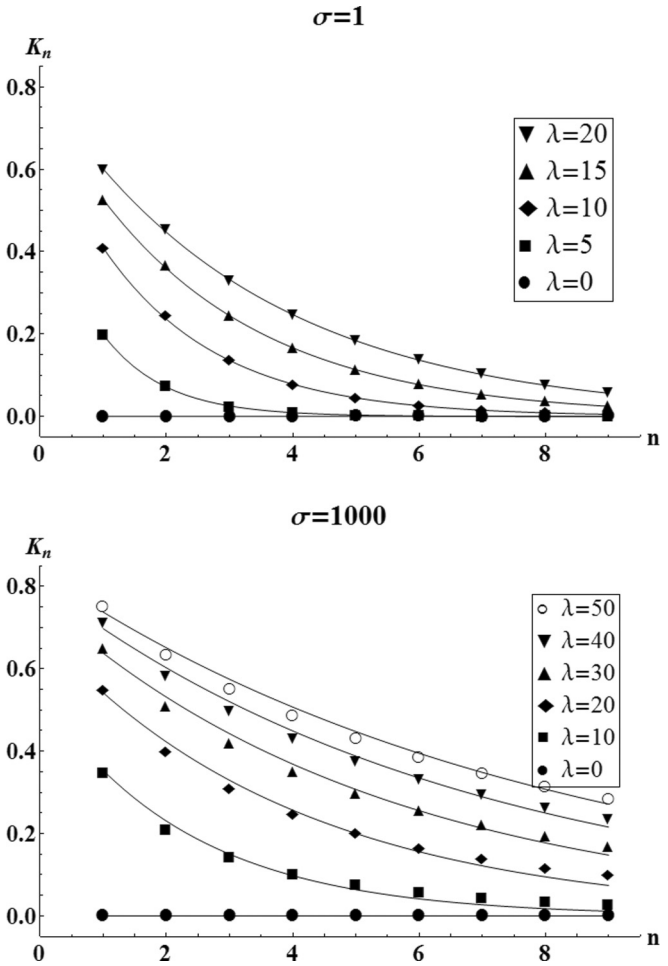

FIG. 4. The synchronization factor K_n for two extreme values of temperature as a function of the beads' distance n. The data have been fitted with the model: $K_n = A_\lambda e^{-B_\lambda n}$.

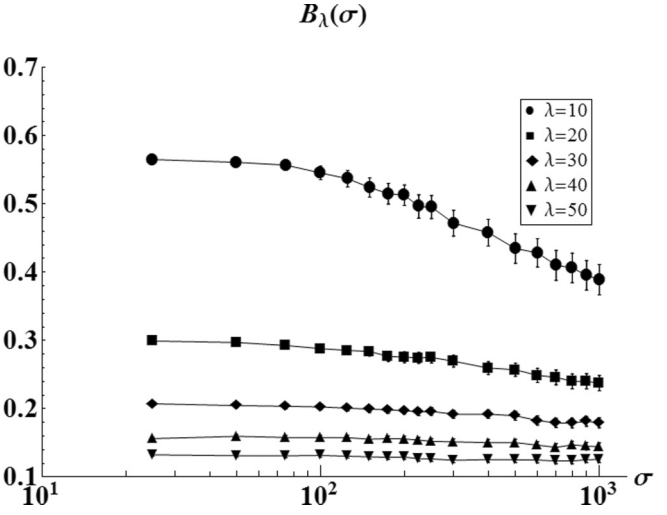

FIG. 5. The synchronization decay factor B_λ as a function of temperature for $\sigma \geqslant 25$.

dominated. According to Fig. 5, the value of B_λ is mainly determined by λ and decreases when the temperature grows by two orders of magnitude. However, for $\lambda \geqslant 30$ this fall is rather insignificant; thus, we conclude that the noise correlation length is the primary factor that influences the effective range of synchronization along the chain.

VII. BEAD MOTION CORRELATION

The other quantities that are also affected by the presence of spatial correlations in noise are the time correlation of the module length and the time correlation of the angles between neighboring modules. These two characteristics describe the time evolution of the chain geometry.

By a module we understand two neighboring beads, so the length of the jth module, at certain moment t, is defined as

$$d_j(t) = |\vec{r}_j(t) - \vec{r}_{j-1}(t)|. \tag{17}$$

The angle between two neighboring modules is defined by the positions of the three following beads:

$$\psi_j(t) = \angle[\vec{r}_{j-1}(t), \vec{r}_j(t), \vec{r}_{j+1}(t)]. \tag{18}$$

With the beginning at the center of the coordinate system, vectors $\vec{r}_i$ are equivalent to the coordinates on a plane; thus they are applied in the above definition. Additionally, one has to remember that the angle ψ_j is directed and varies from 0° to 360° (with 180° indicating that three beads are exactly in line), so the angles have to be measured in a unified way along the whole chain, conserving the initial numeration of beads.

The time correlation function of angles has been calculated in a following way:

$$C_\psi(\tau) = \frac{1}{C_\psi} \sum_{k=0}^{T} \sum_{j=2}^{N-1} [\psi_j(t_k + \tau) - \langle\psi\rangle][\psi_j(t_k) - \langle\psi\rangle]. \tag{19}$$

Here, we introduce the additional summation over j due to the fact that we have $N - 2$ angles for a single moment t, which allows us to increase statistics and obtain a correlation measure for a whole chain, rather than a single site. The normalization factor C_ψ has been chosen as

$$C_\psi = \sum_{k=0}^{T} \sum_{j=2}^{N-1} [\psi_j(t_k) - \langle\psi\rangle]^2, \tag{20}$$

which means that $C_\psi(0) = 1$. Finally, $\langle\psi\rangle$ reads

$$\langle\psi\rangle = \frac{1}{T(N-2)} \sum_{k=0}^{T} \sum_{j=2}^{N-1} \psi_j(t_k). \tag{21}$$

In a strict analogy to the angle correlation function $C_\psi(\tau)$, we can define the module length correlation function $C_d(\tau)$:

$$C_d(\tau) = \frac{1}{C_d} \sum_{k=0}^{T} \sum_{j=2}^{N} [d_j(t_k + \tau) - \langle d\rangle][d_j(t_k) - \langle d\rangle]. \tag{22}$$

C_d and $\langle d\rangle$ are defined similarly to their angle counterparts.

An example of collected data is presented in Fig. 6. In the high temperature regime (approximately for $\sigma > 200$), both $C_\psi(\tau)$ and $C_d(\tau)$ are positive functions, asymptotically falling from 1 to 0, which is typical of stochastic motion. However, they differ significantly in the low temperature regime. While $C_\psi(\tau)$ preserves its high temperature profile (but with values much closer to 1), $C_d(\tau)$ resembles a linear function, falling

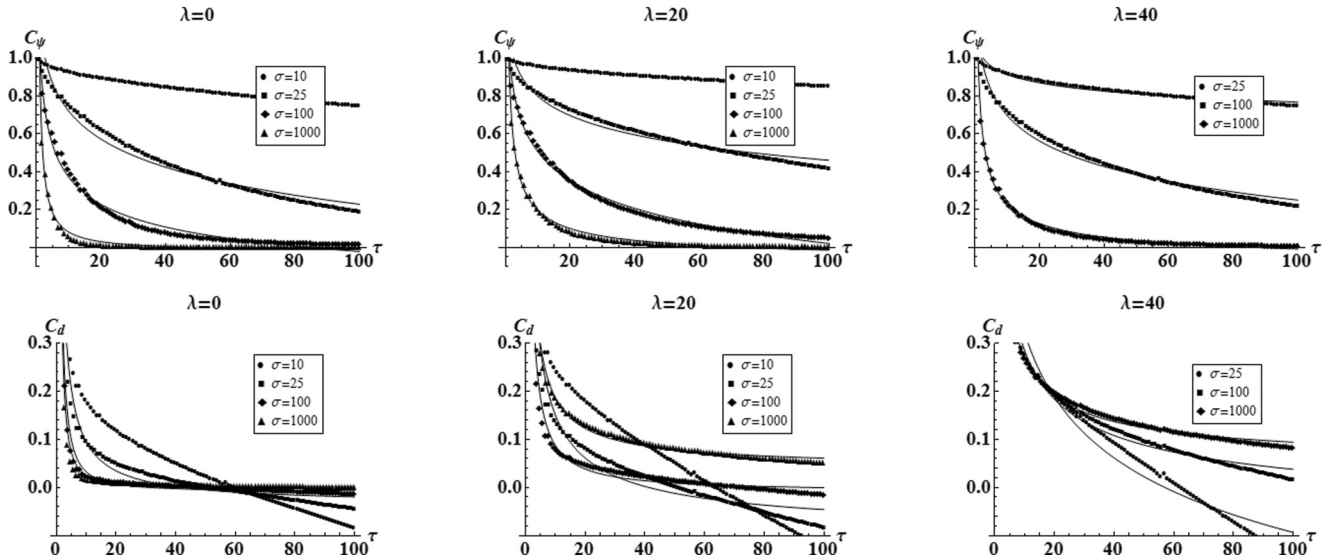

FIG. 6. A representative selection of the module length correlation functions $C_d(\tau)$ and the correlation functions of the angles between neighboring modules $C_\psi(\tau)$. Profiles have been fitted with the function $a\tau^\alpha + c$.

below 0 with the increase in τ. This long-term behavior of the low-temperature $C_d(\tau)$ indicates the domination of the deterministic motion in this temperature regime. In the context of the energetic landscape, introduced in Sec. IV, we can suppose that the beads are trapped at the bottom of their potential energy wells and perform the damped oscillations, slightly perturbed by the noise. Apparently, while the bead motion makes d_j oscillate, it barely affects the angles, so the values of $C_\psi(\tau)$ are relatively close to 1. Additionally, the comparison between $C_\psi(\tau)$ and $C_d(\tau)$ suggests that the module length behavior evolves from deterministic into purely stochastic as the temperature grows, while $\psi_j(t)$ is of a stochastic nature for all σ.

In order to measure the influence of σ and the noise correlation length λ on $C_\psi(\tau)$ and $C_d(\tau)$, we have fitted the profile functions with the following model:

$$C(\tau) = a\tau^\alpha + c. \tag{23}$$

Despite the inaccuracy for $\tau \to 0$ and a divergence in the low-temperature regime, the power function model provides quantitative information on the σ and λ dependencies, thanks to the α parameter. The values of α_d and α_ψ plotted against σ and λ are shown in Fig. 7. As expected, for all values of σ and λ, α is negative and tends to 0 with the decrease in temperature. However, for constant λ, α_ψ decreases at a similar pace with the growth of σ, while α_d varies slowly for most of the temperature range but jumps rapidly below $\sigma = 100$.

The increase in the noise correlation length λ affects both α_d and α_ψ in a similar way, namely, the larger λ is, the lower the $|\alpha|$ obtained is. This means that the correlation functions $C_\psi(\tau)$ and $C_d(\tau)$ decrease at a slower rate, so $d_j(t)$ and $\psi_j(t)$ vary less rapidly over time. Therefore, the dynamics of the chain's shape becomes attenuated, and a current conformation is preserved longer.

VIII. MODULE LENGTH DISTRIBUTION

We have also investigated the marginal distribution $\Gamma(d)$ of the module length d and its temperature evolution, with and without spatial correlations in noise. Taking into account that $d_j(t)$ may express an oscillatory behavior, we have reduced the time interval between data acquisitions to 1/4 of a time unit to avoid synchronization effects. The spatial resolution of histograms has been set to 0.21 length unit.

The profile of $\Gamma(d)$ proved to be a single peaked distribution, concentrated in the vicinity of its mean, with slight, but noticeable, asymmetry. Therefore, in order to describe $\Gamma(d)$ we have calculated its first moment, second central moment (presented in Fig. 8), and the skewness.

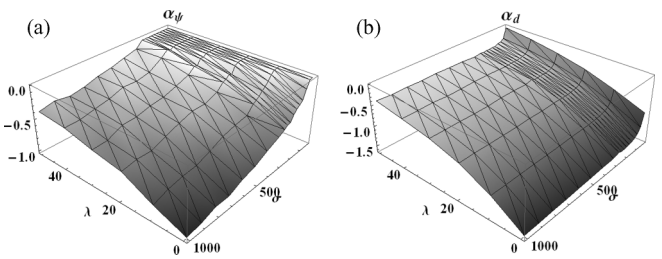

FIG. 7. The exponents (a) α_d and (b) α_ψ resulting from fitting the power function to correlation profiles $C_d(\tau)$ and $C_\psi(\tau)$.

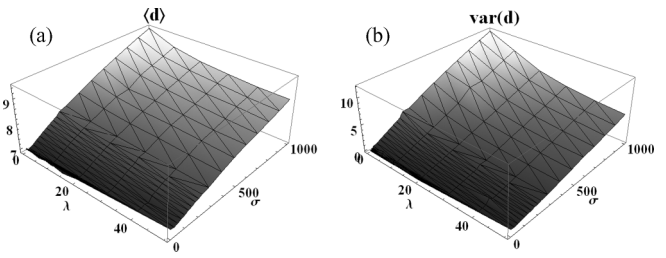

FIG. 8. Statistical characteristics of the module length distribution $\Gamma(d)$ as functions of the noise correlation length λ and the temperature σ: (a) the mean module length $\langle d \rangle$ and (b) the variance of $\Gamma(d)$.

The skewness grows with σ from 0 to approximately 0.6 and saturates at this value. Fortunately, the asymmetry proved to be small enough, so the other parameters are still physically meaningful. The dispersion of distribution $\Gamma(d)$ grows with increasing σ [Fig. 8(b)], which is expected diffusive behavior, but the mean distance $\langle d \rangle$ also tends to grow [Fig. 8(a)], starting from $\langle d \rangle \approx d_0$. This fact, along with the nonzero skewness, indicates that the underlying potential is asymmetric, and, indeed, the presence of the repulsive Lennard-Jones core provides the reflective barrier preventing two neighboring beads from closing up. Conversely, the lengthening of d_j is still possible as the energy well is not as steep for $d_j > d_0$ as in the opposite situation.

The spatial correlations in noise play an inhibitory role for the process of the temperature dependent broadening of $\Gamma(d)$. Here $\lambda \neq 0$ slows down the growth of both $\langle d \rangle$ and the dispersion of $\Gamma(d)$. This effect can be explained by the following reasoning. When a thermal bath imposes noncorrelated, stochastic forces on beads j and $j+1$, this commonly results in a nonzero relative force stretching (or shrinking) the module. However, when the noise is spatially correlated, stochastic forces applied to beads become similar at the length scale of λ, which significantly reduces the relative forcing, and in turn, d is less affected by the noise.

IX. POLYMER UNFOLDING

The most unexpected effect that stems from the presence of the spatial correlations in the noise is the spontaneous linearization of the chain. Having defined angles $\psi_j(t)$ in (18), we have been able to obtain a marginal distribution of angles $\Phi(\psi)$ depending on temperature σ and correlation length λ. Similar to the previous section, the data have been collected every $1/4$ of a time unit, with the resolution of the histogram set to 1°. The representative selection covering the entire range of tested parameters is presented in Fig. 9.

The temperature evolution of distribution $\Phi(\psi)$ gives an insight into how the angular degrees of freedom are freed with the rise in temperature. Let us analyze the $\lambda = 0$ case first. For low temperatures ($\sigma < 10$) we obtain a symmetric bimodal distribution, which is in accordance with the predictions of the double-minimum energetic landscape. However, for extremely low temperatures ($\sigma < 3$) one can see four distinct peaks, which indicates that, probably, there are two additional minima. We can suppose that they are shallow, as they disappear quickly with the rise in σ. For temperatures from $\sigma = 5$ to $\sigma = 13$ the increased penetration of the energy barrier region is noticeable, and the third peak appears exactly at $\psi = 180^\circ$. At $\sigma = 13$ the two peaks indicating energy minimums can no longer be distinguished, and from then on, the shape of the distribution gradually transforms from a bell-like curve into a triangle profile, which is completed approximately for $\sigma = 100$. After that, the distribution broadens systematically with the increase in temperature.

The introduction of $\lambda \neq 0$ affects $\Phi(\psi)$ in a subtle, but remarkable, way. In the low noise regime ($\sigma < 25$) the increase in λ retards the temperature evolution of $\Phi(\psi)$, so the bimodal profile is preserved in a wider interval of σ. However, when σ exceeds 50, the profile transforms into a heavy-tailed peaked

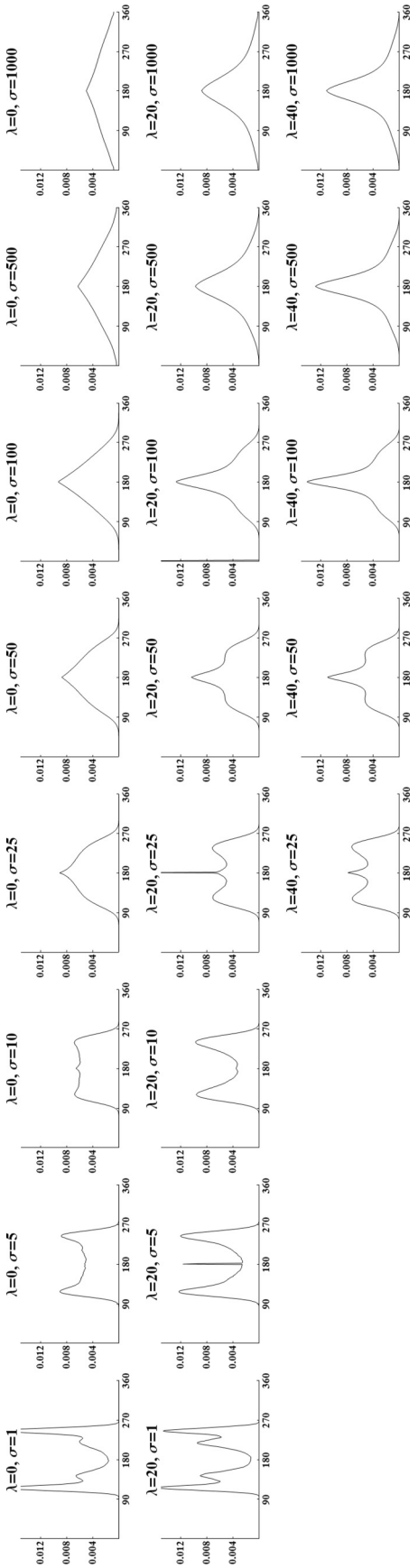

FIG. 9. The temperature evolution of angle distribution $\Phi(\psi)$ for noise correlation length $\lambda = 0$, $\lambda = 20$, and $\lambda = 40$.

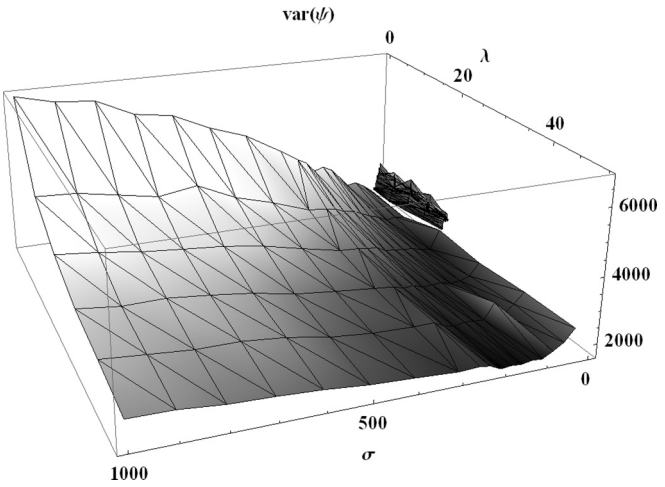

FIG. 10. The dispersion of distribution $\Phi(\psi)$ as a function of the noise correlation length λ and the temperature σ.

distribution, much more concentrated in the vicinity of $\psi = 180^\circ$ than in the case of $\lambda = 0$. The dispersion of $\Phi(\psi)$ is a measure of this effect, which shows that the higher λ is, the lower the value of $\Phi(\psi)$'s second central moment is. This indicates the linearization of the chain and thus its unfolding. This is illustrated in Fig. 10.

The single-peaked distribution with $\langle\psi\rangle = 180^\circ$ indirectly suggests that for high temperatures the system selects the single-minimum energetic configuration similar to the one shown in Fig. 2(b) rather than the double-minimum landscape in Fig. 2(a). Knowing that the growth of the distance $l_j = |\vec{r}_{j+1} - \vec{r}_{j-1}|$ is a crucial factor in the merging of energetic minima, we can suppose that l_j is subject to interplay similar to d_j, namely, the repulsive cores do not allow beads $j-1$ and $j+1$ to close up, while the stretching of l_j is still possible. With sufficiently high noise, this asymmetry could lead to the rise in $\langle l\rangle$ and the domination of the single-minimum potential topology. This transition seems inherent to the system, and it is present regardless of the spatial correlations in noise. Nevertheless, once the single-minimum state prevails, the bead can explore the well, provided there is enough relative forcing, and for $\lambda \neq 0$ this forcing drops dramatically. As a result, despite the high noise amplitude, the bead is trapped near the minimum, so the angles between modules cannot vary as much as in the noncorrelated case. This leads to a narrowing of $\Phi(\psi)$ around $\psi_j = 180^\circ$.

X. SUMMARY

Summarizing our research, the most salient conclusion one can draw is that spatial correlations in thermal noise have an overall inhibitory effect on the system. This manifests in the general attenuation of the chain geometry dynamics both in the time domain, where the polymer tends to preserve its current shape, and in the temperature domain, where the evolution of the statistical chain properties is retarded. It is also in agreement with our previous findings that the presence of nonzero correlations reduced the ability of the chain to transfer between different conformations [13].

Such a behavior is not a surprise, as we can perceive the introduction of the spatial correlations into the thermal bath as a freezing of environment, and in the limit $\lambda \to +\infty$, this should also lead to the complete attenuation of the system dynamics. In this context, it is not solely the temperature of the thermal bath that influences the system behavior but also the structure of the environment. Our approach, which decouples the temperature from the environmental correlation length, allows for more plasticity than the explicit simulation of thermal bath particles but requires proper scaling to avoid unphysical situations.

[1] F. Sagués, J. M. Sancho, and J. García-Ojalvo, Rev. Mod. Phys. **79**, 829 (2007).
[2] R. Morgado, M. Cieśla, L. Longa, and F. A. Oliveira, Europhys. Lett. **79**, 10002 (2007).
[3] C. W. Gradiner, *A Handbook of Stochastic Processes*, 3rd ed. (Springer, Berlin, 2004).
[4] S. C. Kou, Ann. Appl. Stat. **2**, 501 (2008).
[5] P. N. Segrè, E. Herbolzheimer, and P. M. Chaikin, Phys. Rev. Lett. **79**, 2574 (1997).
[6] E. Guazzelli, Phys. Fluids **13**, 1537 (2001).
[7] P. T. Underhill, J. P. Hernandez-Ortiz, and M. D. Graham, Phys. Rev. Lett. **100**, 248101 (2008).
[8] J. J. Binney *et al.*, *The Theory of Critical Phenomena* (Oxford University Press, Oxford, 1992).
[9] M. Mosayebi, E. Del Gado, P. Ilg, and H. C. Öttinger, Phys. Rev. Lett. **104**, 205704 (2010).
[10] C. Donati, S. C. Glotzer, P. H. Poole, W. Kob, and S. J. Plimpton, Phys. Rev. E **60**, 3107 (1999).
[11] B. Doliwa and A. Heuer, Phys. Rev. E **61**, 6898 (2000).
[12] A. C. Mitus, A. Z. Patashinski, A. Patrykiejew, and S. Sokolowski, Phys. Rev. B **66**, 184202 (2002).
[13] M. Majka, P. F. Góra, Acta Phys. Pol. B **43**, 1133 (2012).
[14] E. Donth, H. Huth, and M. Beiner, J. Phys. Condens. Matter **13**, L451 (2001).
[15] C. Dalle-Ferrier, C. Thibierge, C. Alba-Simionesco, L. Berthier, G. Biroli, J. P. Bouchaud, F. Ladieu, D. L'Hôte, and G. Tarjus, Phys. Rev. E **76**, 041510 (2007).
[16] E. R. Weeks, J. C. Crocker, and D. A. Weitz, J. Phys. Condens. Matter **19**, 205131 (2007).
[17] R. Kubo, M. Toda, and N. Hashitsume, *Statistical Mechanics II* (Springer, Berlin, 1985).
[18] G. H. Golub and C. F. Van Loan, *Matrix Computations* (Johns Hopkins University Press, Baltimore, 1996).
[19] R. Wieczorkowski and R. Zieliński, *Komputerowe generatory liczb losowych* (WNT, Warsaw, 1997).
[20] N. G. van Kampen, *Stochastic Processes in Physics and Chemistry* (Elsevier, Amsterdam, 1987).
[21] P. E. Kloeden and E. Platen, *Numerical Solutions of Stochastic Differential Equations*, 3rd ed. (Springer, Berlin, 1999).